Available online at www.sciencedirect.com

jmr&t Journal of Materials Research and Technology

journal homepage: www.elsevier.com/locate/jmrt

High strain-rate deformation analysis of open-cell aluminium foam

Anja Mauko [a,*], *Mustafa Sarıkaya* [b], *Mustafa Güden* [b], *Isabel Duarte* [c,d], *Matej Borovinšek* [a], *Matej Vesenjak* [a], *Zoran Ren* [a]

[a] *Faculty of Mechanical Engineering, University of Maribor, Maribor, Slovenia*
[b] *Dynamic Testing and Modeling Laboratory and Department of Mechanical Engineering, Izmir Institute of Technology, Gülbahçe Köyü, Urla, Izmir, Turkey*
[c] *Department of Mechanical Engineering, TEMA, University of Aveiro, Campus Universitário de Santiago, Aveiro, Portugal*
[d] *LASI - Intelligent Systems Associate Laboratory, Portugal*

ARTICLE INFO

Article history:
Received 11 April 2023
Accepted 31 May 2023
Available online 3 June 2023

Keywords:
Open-cell aluminium foam
Micro-computed tomography
High-strain rate
Direct impact hopkinson bar
Digital image correlation
Computer simulation

ABSTRACT

This study investigated the high-strain rate mechanical properties of open-cell aluminium foam M-pore®. While previous research has examined the response of this type of foam under quasi-static and transitional dynamic loading conditions, there is a lack of knowledge about its behaviour under higher strain rates (transitional and shock loading regimes). To address this gap in understanding, cylindrical open-cell foam specimens were tested using a modified Direct Impact Hopkinson Bar (DIHB) apparatus over a wide range of strain rates, up to 93 m/s. The results showed a strong dependency of the foam's behaviour on the loading rate, with increased plateau stress and changes in deformation front formation and propagation at higher strain rates. The internal structure of the specimens was examined using X-ray micro-computed tomography (mCT). The mCT images were used to build simplified 3D numerical models of analysed aluminium foam specimens that were used in computational simulations of their behaviour under all experimentally tested loading regimes using LS-DYNA software. The overall agreement between the experimental and computational results was good enough to validate the built numerical models capable of correctly simulating the mechanical response of analysed aluminium foam at different loading rates.

1. Introduction

Studying cellular materials is a crucial area of modern engineering materials research since they possess advanced mechanical properties such as high stiffness at low-density, high-energy absorption, and thermal and electrical conductivity. Especially mechanical response of metallic cellular materials is widely studied in the scientific community [1]. The mechanical behaviour of a material can be highly dependent on the strain rate, making comprehensive characterisation of materials across all loading regimes essential [2–4]. Three strain rate loading regimes are usually identified: quasi-static, transitional dynamic, and shock [5]. A quasi-

* Corresponding author.
E-mail address: anja.mauko@um.si (A. Mauko).
https://doi.org/10.1016/j.jmrt.2023.05.280

static regime dictates the deformation of the material, where the response is mainly governed by force equilibrium, negating the effect of inertia. Quasi-static test results often serve as a foundation for evaluating and comparing changes in the deformation modes at different strain rates. With increasing strain rate, the influence of inertia starts to dominate, leading to altered deformation behaviour and enhanced mechanical properties [6]. Cellular materials exhibit localised deformation, and stress increases at high loading rates due to the influence of inertia, which is particularly evident in the shock regime [7].

Despite the growing interest in cellular materials, much of the research has been focused on their characterisation only under quasi-static loading conditions [8]. While some studies have attempted to study these materials under dynamic conditions [9,10], these have been mainly limited to computational simulations. In our previous investigation [11], the open-cell foam specimens were scanned using the X-ray micro-computed tomography (mCT) and computationally reconstructed to analyse the effects of the real internal cellular structure on their mechanical behaviour. Comparing results with theoretical geometry predictions showed significant differences and proved the importance of precise modelling of the inner structure. The 3D Voronoi tessellation method and beam modelling were also employed to reproduce the irregular open-cell internal structure for numerical models used in impact computer simulations [12]. The computational results indicated a decrease in Young's and increased tangent modulus due to more significant cell shape irregularity of the model. The same open-cell foam was computationally and experimentally analysed at lower loading rates in Ref. [13], which revealed small strain rate sensitivity and micro inertia effects. Recent study on similar open-cell material aimed to investigate the effect of biaxial combined compression-torsion loading complexity on the mechanical properties of aluminium foams with different porosities [14]. The results showed that higher foam density and increased loading complexity resulted in improved yield strength, energy absorption capacity, and micro-hardness. Most recent study on open-cell aluminium aluminium foam at high impact velocities characterised the material by using the numerical simulations [15]. Therefore, a model of the open-cell foam based on Voronoi tessellation was created, allowing for the prediction of stress, strain, and energy dissipation characteristics. The results demonstrated a strong correlation between the computational predictions and theoretical expectations, affirming the accuracy of the method in assessing the shock-wave mechanical behaviour. The general lack of the complete experimental characterization in all loading regimes can be observed from the most recent review publication on foam materials [16].

One commonly used method for testing materials under fast dynamic loading is the Split Hopkinson Pressure Bar (SHPB) test apparatus [17,18]. In study [19], the researchers used an SHPB apparatus to characterise a similar open-cell material that functioned as the core component of a sandwich structure. The primary emphasis of the study was on characterizing deflection profiles. However, it is important to note that the properties assessed in the study were solely obtained for the sandwich structure and not for the open-cell material such. The open-cell Duocel® material [20] was also characterised using an SHPB apparatus at strain rates up to 4580 1/s. However, it was only possible to achive a maximum strain of 0.4 due to the samples material's low impedanc. As a result, a full characterization of the complete deformation behaviour was not achieved. Similary, other researchers have encountered certain limitations when using this method to study cellular materials related to their low impedance and stress wave dispersion, highlighted in studies [4,21,22]. The SHPB method also has a limited deformation and strain rate range, depending on the size of the apparatus. The test results of cellular materials obtained from classical SHPB experiments are also limited due to cellular structure effects. The Digital Image Correlation (DIC) method must be used to avoid irregularities. To overcome these limitations, upgraded versions of the apparatus, such as the Open Hopkinson Pressure Bar [23] and the Direct Impact Hopkinson Bar (DIHB) [24,25], have been proposed. This study aimed to comprehensively characterise the open-cell aluminium foam M-pore® under various strain rate loading regimes with use of recently modified DIHB apparatus for the first time. As discussed in the preceding paragraphs, the application of open-cell foam M-pore® at lower strain rates has already been investigated. However, to achieve a comprehensive understanding of the properties of open-cell materials, a modified DIHB apparatus was utilised to facilitate characterization at strain rates relevant to shock conditions until full densification. The presented approach combines experimental characterization using the DIHB apparatus and the DIC method, which has not been previously employed for the specific material under investigation. Furthermore, developed numerical models were verified by experimental testing. The models can thus be used in computational simulations to estimate the material behavior and properties also at strain rates not achieved by used available experimental techniques. Experiments were performed at a wide range of impact velocities using both quasi-static and dynamic testing methods. The quasi-static experiments were conducted using a traditional compression Instron device, while the dynamic experiments were performed using a modified DIHB set-up. The initial impact velocities were determined using the Rigid Power Low Hardening (R-PLH) constitutive model, which accurately defined the critical velocities separating the different loading regimes. Additionally, the DIHB results were used to validate the numerical model used for computational simulations based on microcomputed X-ray tomography (mCT) of tested specimens.

2. Methodology and material

2.1. *Specimen fabrication*

The open-cell aluminium foam specimens were fabricated by M-pore® GmbH using a casting method that uses a polymer foam as a starting material [26]. The polymer foam was converted into an open-cell structure through reticulation treatment and filled with heat-resistant material. The polymer was then melted away by the heat. The resulting cellular mould was then filled with molten aluminium EN AW-1070 (DIN

Al99.7). Lastly, the mould was removed by applying high pressure, resulting in an open-cell aluminium foam plate. The foam plate was then cut into cylindrical specimens with dimensions of Ø19 mm × 20.5 mm (Fig. 1) using an electro-discharge machine (EDM). The main mechanical properties of open-cell M-pore® specimens used in quasi-static experiments are listed in Table 1. Parameters m and ρ represent the mass and density of the specimen. The average porosity (p) of the prepared foam specimens is 93.9%. The plate was colour marked on one side before cutting to ensure consistent loading orientation for all specimens during subsequent experimental testing.

2.2. X-ray micro-computed tomography

The open-cell aluminium foam specimens were scanned using an X-ray mCT equipment from SkyScan 1275 (Bruker mCT, Kontich, Belgium) with an X-ray beam of 50 kV and 200 μA. The equipment had a resolution of 14 μm, an exposure time of 75 ms, and 5 frame averaging. The rotation step was set at 0.3°, with a 1 mm Al filter and a full rotation of 360°. The X-ray detector used a 3 MP (1944 px × 1536 px) active pixel CMOS flat panel. The NRecon (v.1.7.3.1 software, Bruker, Kontich, Belgium), CTVox (v.3.3.0 r1403 software, Bruker, Kontich, Belgium), and CTAn (v.1.17.7.2 software, Bruker, Kontich, Belgium) software were used to reconstruct cross-section slices from the acquired 2D angular projections, perform 3D-reconstruction, and analyse the morphometric properties such as porosity and cell size distribution, respectively.

2.3. Experimental testing

Experiments were conducted across various strain rates, encompassing all three main loading regimes: quasi-static, transitional dynamic, and shock [27].

Fig. 1 – M-pore® open-cell aluminium specimen.

Table 1 – Mechanical properties of open-cell M-pore® specimens.

Specimens no.	m [kg]	ρ [kg/m^3]	p [%]
S1	0.98	171.73	93.6
S2	0.89	155.46	94.2
S3	0.91	158.88	94.1
S4	0.96	165.66	93.8
S5	0.93	161.80	94.0
Average	0.93	162.71	93.9

2.3.1. Quasi-static loading

The basic material properties of the aluminium foam specimens were determined using a compression test on an INSTRON 8801 device at the Faculty of Electrical Engineering, Mechanical Engineering and Naval Architecture at the University of Split, Croatia [1]. The maximum loading force was set to 30 kN at a loading rate of 0.1 mm/s. Five tests (S1–S5) were conducted to ensure repeatability due to the non-homogenous structure of the aluminium foam specimens. All test specimens were scanned using mCT equipment to determine the internal structure before the quasi-static experiments, which was crucial for the development of specimen geometry in computational models.

2.3.2. Dynamic loading

2.3.2.1. *DIHB experiments*. The high-speed experiments were carried out using a DIHB testing device at the Dynamic Testing and Modelling Laboratory and Department of Mechanical Engineering, Izmir Institute of Technology, Turkey [28]. The DIHB set-up consisted of an incident bar that was 3110 mm long and had a diameter of 19.4 mm. Table 2 lists the mechanical properties of the incident bar steel Inconel 718, where E, ν, ρ, $R_{p\,0.2}$ and R_m represent the Youngs modulus, Poisson's ratio, density, yield, and tensile strength.

Impact experiments were conducted at five different impact velocities of 14, 26, 56, 76, and 94 m/s to study the strain rate effect on open-cell aluminium foam. Different impact velocities were achieved by using different striker materials and adjusting the acceleration pressure. At lower velocities (14 and 26 m/s), an Inconel 718 striker was used. Wooden strikers were utilised to achieve higher velocities. All strikers were 200 mm in length. The wooden strikers were only used for achieving high-strain rates and were therefore regarded as a rigid body within the scope of this study. This assumption is justified by the observed course of deformation propagation under shock loading conditions. In this mode, deformation initiates at the point of impact and progressively spreads towards the opposite end. Previous studies [28] have already established this phenomenon, which was further corroborated by the analysis of digital images captured during the experiments. Consequently, the shock wave does not reach the striker until the deformation process of the sample is fully concluded. The wooden strikers were made of dry red

Table 2 – The mechanical properties of the Inconel 718.

E [GPa]	ν [/]	ρ [kg/m^3]	$R_{p\,0.2}$ [MPa]	R_m [MPa]
207	0.29	7800	1100	1375

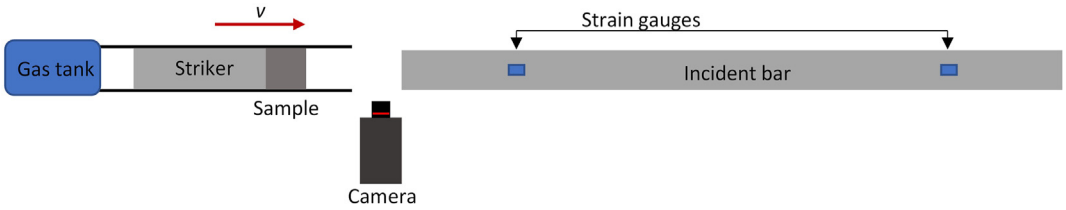

Fig. 2 – Schematic of the DIHB testing set-up.

oak with modulus of elasticity 57,000 MPa and compression strength parallel to grain 23.9 MPa.

The specimen was attached to the striker, which served as the backing mass, and accelerated towards the incident bar by releasing pressure from a gas tank. The experiments mimic the principle of the Taylor test, where specimens are accelerated into a rigid wall. The specimen deformation during impact with the incident bar was recorded using a high-speed camera, Photron Fastcam SA-Z, at 100,000 fps with a resolution of 302 px × 128 px. Its primary purpose was to accurately determine the initial impact velocity, velocity profiles, and the propagation of the deformation front.

The incident bar was equipped with strain gauges at two different positions, as shown in Fig. 2. The first measuring point was 1460 mm from the impact end, and the second was 2110 mm from the impact end. The acquisition of experimental results at two measuring locations was crucial for separation of the propagating deformation waves in the incident bar. The strain gauges at each point were connected to a full Wheatstone bridge circuit. The voltage output V_o in each Wheatstone bridge was measured and amplified to compensate for the low amplitude of the outgoing signal during the experiments. The engineering strain at both measuring points in the incident bar was then determined as [29]:

$$\varepsilon_T(t) = \frac{2V_o}{G_f A_g (1+\nu)(V_E - V_o)} \tag{1}$$

where the excitation voltage was $V_E = 10$ V, strain gauge factor $G_f = 2.09$, amplification $A_g = 200$ and Poisson's ratio $\nu = 0.29$.

The impact between the specimen and the incident bar creates a deformation wave that propagates along the incident bar. When this wave reaches the free end of the bar, it is reflected and travels back as a tensile wave. The superposition of these two waves creates inaccuracies in measuring the propagating strain on the incident bar. To eliminate this overlap, the method of strain wave separation was used, as proposed by Lie et al. [21].

The mechanical properties of the open-cell aluminium foam were analysed using the results from the strain measurements converted to engineering stress. First, the highest Peak Stress (PS) before the plateau stress was evaluated. The plateau region was characterised by two significant parameters: the plateau stress σ_p, which is the average stress value between 0.2 and 0.4 strain, and the densification stress σ_d, which is calculated as 1.3 times the plateau stress. The densification strain ε_d corresponds to the densification stress σ_d. The Specific Energy Absorption (SEA) of the specimens until densification strain ε_d was evaluated as:

$$SEA = \frac{\int_0^x F\,dx}{m} \tag{2}$$

where F represents the force and m represents the mass of the specimen.

2.3.2.2. Digital image correlation (DIC). High-speed camera was used to capture digital images of all dynamic experiments, and the recorded deformation sequence was saved in a PNG format without compression. The DIC method was employed to analyse the recorded digital images to evaluate experimental results. The DIC method involves tracking the movement of reference pixels in an image sequence, with the first image taken just before the impact of the specimen and incident bar. The exact values of specimen deformation and impact velocity were determined by using a subset of each reference pixel and the known image resolution and sampling frequency of the high-speed camera by using Matlab scripts written by the Czech Academy of Sciences' Institute of Theoretical and Applied Mechanics [2,30].

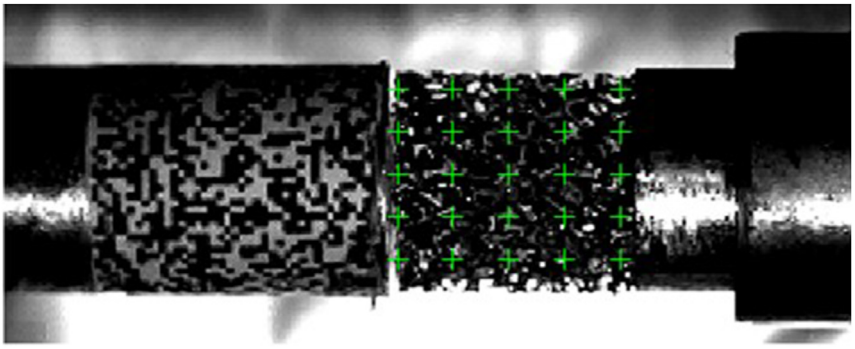

Fig. 3 – DIC method evaluation of the initial impact velocity.

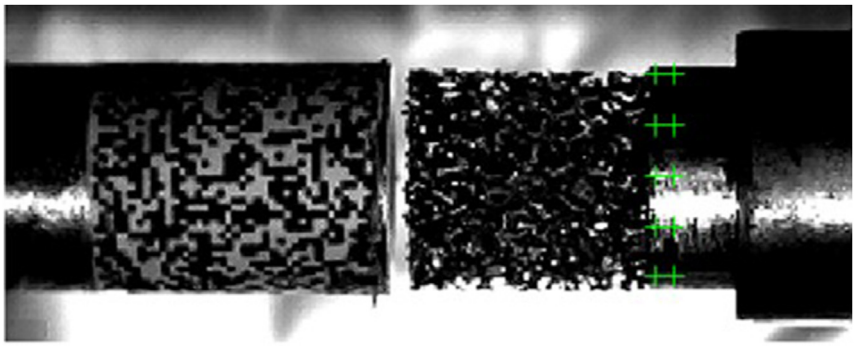

Fig. 4 – DIC method evaluation of the velocity profiles.

The initial impact velocity was at first determined by the two-laser method [10]. However, it was found to overestimate the actual impact velocity, particularly at higher velocities, due to the indirect measurement of the two-laser method at some distance away from the impact location. The DIC method was therefore used for all velocity evaluations in the conducted experiments using correlation images taken just before the impact to ensure the precise determination of the impact velocities. The correlation points, represented by green crosses, were positioned on the undeformed specimen, as shown in Fig. 3. The red arrow indicates the specimens' and strikers' movement direction. The impact velocity was calculated by measuring the displacement between the second-to-last and last image taken before the impact. The impact was defined as the first point of contact between the specimen and the incident bar.

The DIC method was also used to determine the striker velocity profile during deformation by measuring the displacement of pixels in an image sequence. Selecting the correct starting image is important to get an accurate velocity profile. The correlation points were placed on the striker end directly after the specimen to accurately represent the true velocity profile, as shown in Fig. 4.

2.4. *Computer simulations*

The Finite Element Method (FEM) and the LS-DYNA software [31] were used for computer simulations reported in this study.

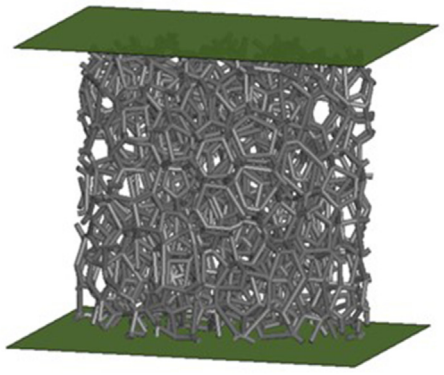

Fig. 5 – Numerical model of open-cell aluminium foam specimen S1.

The simulation models consisted of three main parts: an upper plate, an aluminium foam specimen, and a bottom plate, as shown in Fig. 5. The specimen was placed between the plates, which were discretised with rigid linear shell finite elements using the Belytschko-Tsay formulation.

Five different specimen geometries S1–S5 were built to account for the inhomogeneity of the cellular foam structure. The geometries of the built numerical models were reconstructed from the fabricated foam specimens by using the mCT images. This allowed a direct comparison between identical structures' experimental and computational results.

Reconstructing the geometry of open-cell aluminium foam specimens began with obtaining mCT images of the fabricated foam specimens. These images were then converted into a grayscale stack made up of voxels, which were then thresholded to separate the foam material (white pixels) from the background (black pixels). A thinning algorithm was applied to the material voxels, resulting in a one-voxel-thick skeleton representing the foam's struts and connections. By assuming that all struts could be modelled as straight lines, the geometry of the aluminium foam was reconstructed [11]. The struts were then converted into a finite element mesh by dividing them into 3 to 5 quadratic beam finite elements, depending on the strut length. The Hughes-Liu beam finite element formulation [23] with a simplified constant circular cross-section was used. The constant diameter of the struts 0.398 mm was calculated by equating the numerical model and fabricated specimen mass. The numerical model of foam specimen S1 is shown in Fig. 5. The struts are neither ideally circular nor with a constant cross-section along their entire length in the real foam specimens. However, the simplified numerical models using beam finite elements allow for very fast parametric computations compared to more precise numerical models with struts discretised using solid finite elements. Previous studies show that the simplified numerical model of foam specimens returns a slightly less stiff response than the real foam specimens.

Table 3 – Mechanical parameters of the open-cell foam base material EN AW-1070.

E [GPa]	ν [–]	ρ [kg/m^3]	$\sigma_{y,qs}$ [MPa]	E_t [MPa]	C [s^{-1}]	p [–]
70	0.35	2700	60	84	6500	4

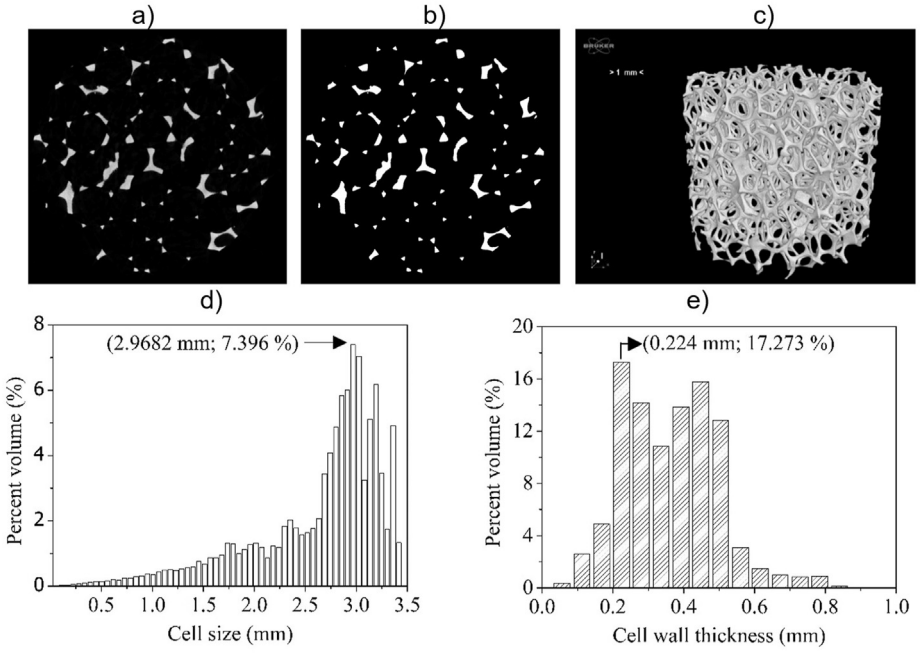

Fig. 6 – a) Grayscale reconstructed 2D image, b) binary 2D image, c) 3D rendered reconstructed foam sample, d) cell size distribution and e) cell wall thickness distribution.

A kinematic plastic material model (MAT_PLASTIC_KINEMATIC_003) was used to simulate the mechanical response of the base material of the foam. The base material parameters (Poisson's ratio, yield stress, and tangent modulus) are given in Table 3. The simulation models also captured the influence of the strain rate by using the Cowper-Symonds constitutive model, defined by the following equation:

$$\sigma_{y,d} = \sigma_{y,qs}\left[1 + \left(\frac{\dot{\varepsilon}}{C}\right)^{1/p}\right] \quad (3)$$

where material parameters $\sigma_{y,d}$, $\sigma_{y,qs}$ and $\dot{\varepsilon}$ represent dynamic yield stress, static yield stress and deformation strain rate. Parameters C and p represent Cowper-Symods coefficient for the considered material. The chosen constitutive model was selected based on previously proven suitability specific for the open-cell foam [32] used in this study.

An AUTOMATIC_GENERAL contact was prescribed to simulate open-cell foam self-contacts as it enables body-to-self contacts that occur during the densification of the cellular material. The contact automatically checks the interference along the entire length of the element. An AUTOMATIC_NODE_TO_SURFACE contact was assumed for the contact between the rigid plates and the foam specimen. A friction coefficient of 0.35 was prescribed at the contacts [33].

The upper plate in the simulation acted as the means of applying load to the open-cell specimen. It was constrained to prevent movement in the lateral direction regarding the specimen. The bottom plate was fixed and immovable in all directions. The displacement measurements were taken on the upper plate, and reaction forces were recorded on the bottom plate.

The numerical models were subjected to compressive loading with the same conditions as the experimental tests.

Table 4 – mCT results obtained using CTAn software.

Percent object volume [%]	Porosity [%]	Cell size [mm]		Cell wall thickness [mm]	
		Average	Standard deviation	Average	Standard deviation
5.94	94.1	2.63	0.642	0.36	0.135

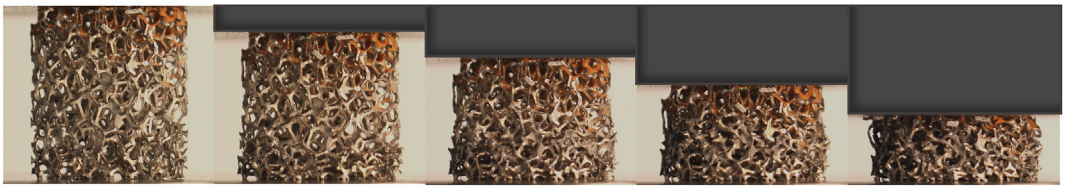

Fig. 7 – Compression behaviour of open-cell specimens under quasi-static loading conditions.

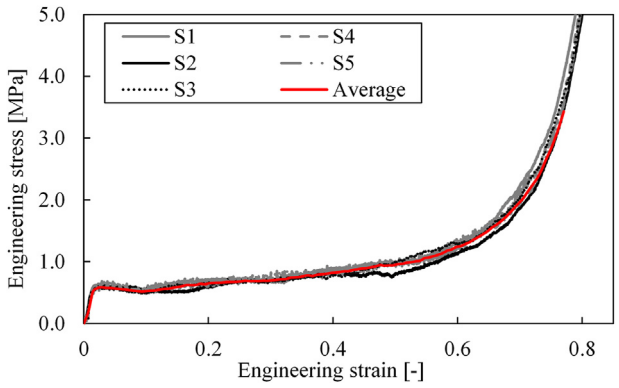

Fig. 8 – Engineering stress-strain relationship of individual experiments and their average value at quasi-static loading regime.

The loading rate for the quasi-static regime was scaled up to 5 s^{-1} for explicit simulations to decrease computation time. Initial tests confirmed that such loading rate upscaling does not affect the accuracy of the results since the inertia influence is negligible.

3. Results

3.1. *X-ray micro-computed tomography*

Fig. 6 demonstrates the process of X-ray mCT image processing, segmentation, and reconstruction of open-cell foam specimens. The segmentation step was crucial in separating the two phases of the specimen (solid and voids), providing the necessary input for the subsequent steps. This was achieved by converting the 2D slices of the grayscale images (Fig. 6a) into binary images (black and white, Fig. 6b) using a Global method. The 3D reconstruction of the foam specimen is seen in Fig. 6c.

The porosity, cell size distribution, and cell wall thickness distribution of analysed foam specimens were determined from the binary images using the CTAn software. The cell sizes were quantified by evaluating the cell volume and calculating the diameter of an equivalent sphere. The morphometric results are summarised in Table 4. The range of cell sizes in the open-cell aluminium foam specimens (porosity of 94.1%, Table 4) varies between 0.056 mm and 3.416 mm (Fig. 6d), with an average of 2.63 mm (Table 4). In contrast, the range of cell wall thickness varies between 0.056 mm and 0.84 mm (Fig. 6e), with an average of 0.36 mm (Table 4).

Table 5 – Initial impact velocities determined by the DIC method.

Test No.	Initial impact velocity [m/s]	Average initial impact velocity [m/s]
1	13.81	14.0
2	14.14	
3	14.15	
4	25.90	25.9
5	54.00	55.7
6	58.00	
7	55.00	
8	76.00	76.0
9	93.61	93.6
10	94.47	
11	92.61	

3.2. *Experimental results*

3.2.1. *Quasi-static loading*

The key indicator of the type of material loading and deformation regime under compression loading is the initial location and spread of the deformation front. For quasi-static loading and deformation regime the first signs of deformation appear at the specimen's weaker points leading to the appearance of typical deformation bands. The compressive deformation progress in the open-cell specimen at a loading rate of 0.1 mm/s is shown in Fig. 7 at a 15% deformation steps.

The results of five quasi-static experiments are illustrated in Fig. 8 as engineering stress-strain relationships, exhibiting a common three stress stage patterns: an initial elastic stage, a prolonged plateau stage with little change in stress despite a significant increase in strain, and a densification stage marked by a sharp increase in stress. Young's modulus was determined to be 40.97 MPa. The elastic deformation persisted until

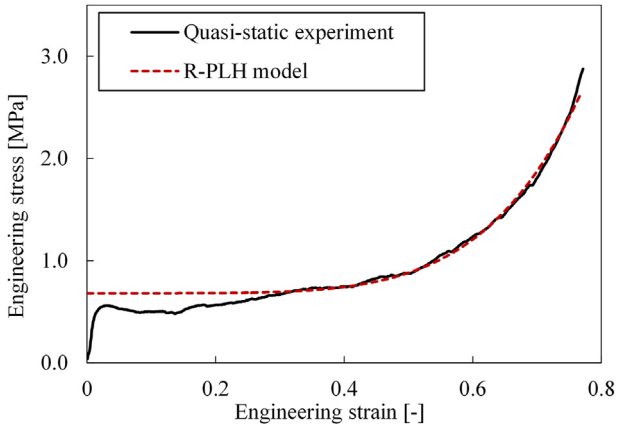

Fig. 9 – Quasi-static experiment and the R-PLH model mechanical response comparison.

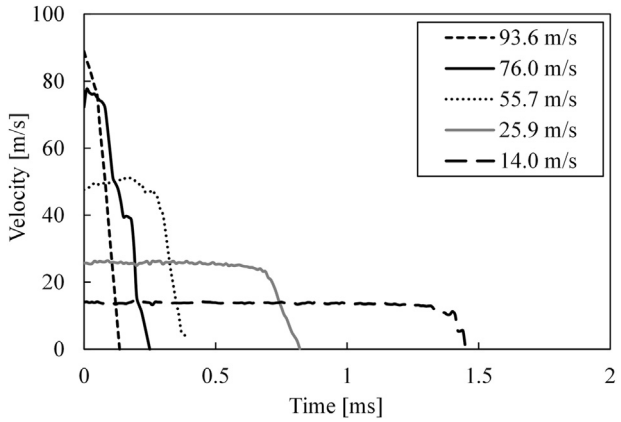

Fig. 10 – Striker velocity profiles after the initial impact.

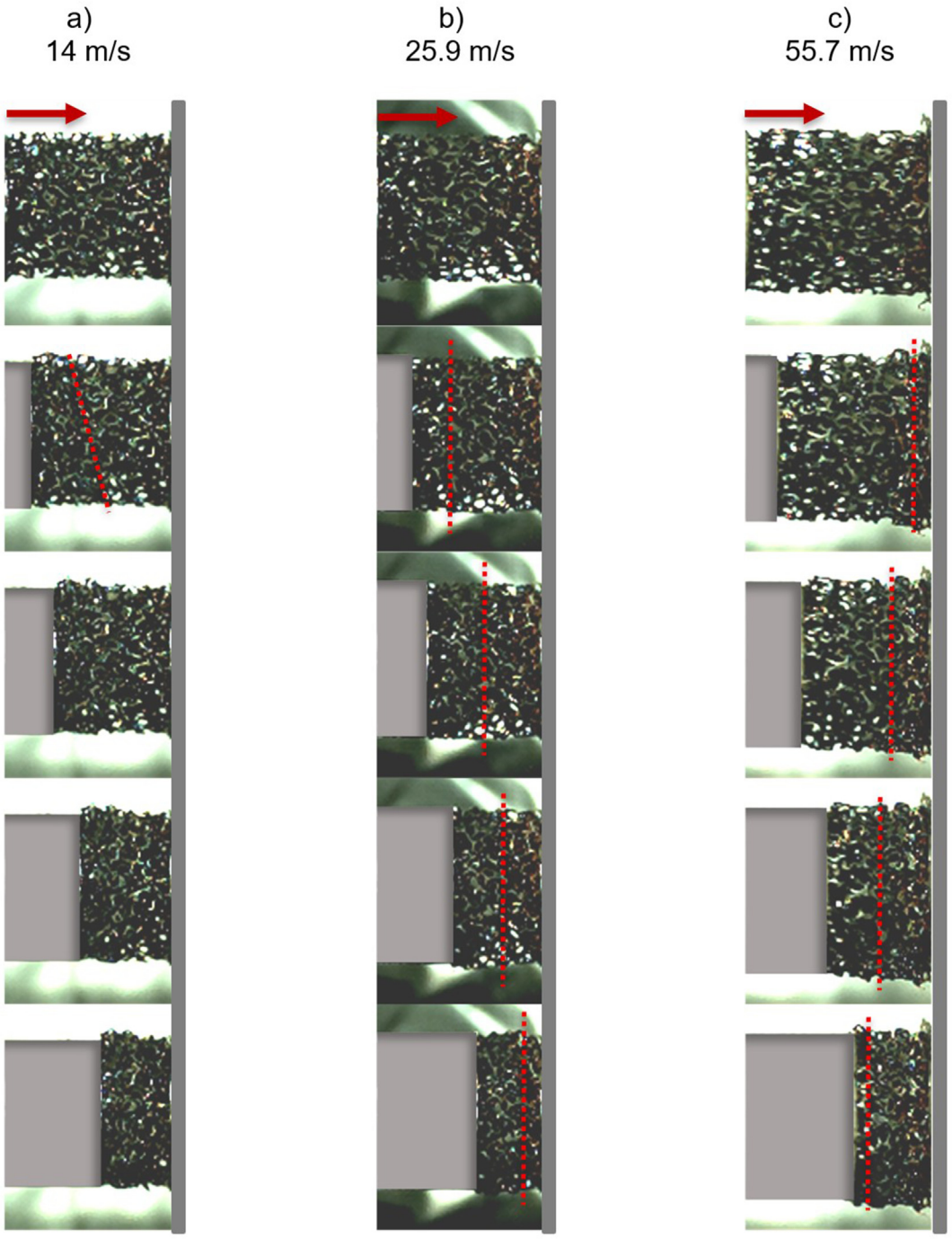

Fig. 11 – Deformation behaviour (deformation step of 15%) with deformation front initiation and propagation in a) quasi-static, b) transitional dynamic, and c) shock loading regime.

the peak stress at 0.58 MPa, followed by a plateau stage with an average stress σ_p of 0.72 MPa. Small, inconsequential stress fluctuations within the plateau region may occur due to random geometry, the unstable deformation of the underlying material, and specimen imperfections. Although the inner structure of the open-cell samples may vary due to differences in the production method, the stress-strain results presented in Fig. 8 demonstrate an almost identical response among the samples. This indicates that the differences in the inner structure of the samples do not significantly affect the stress-strain behaviour. Therefore, it can be concluded that the observed variations in microstructure do not have a substantial impact on the stress-strain results. The densification stage was reached at a strain ε_d of 0.5 and a stress σ_d of 0.93 MPa. The SEA was evaluated to be 2.08 J/g. The quasi-static testing results were used as input data for the R-PLH

model utilised to predict critical impact velocities of evaluated aluminium foam specimens.

3.2.1.1. R-PLH model prediction of critical impact velocities. Two critical impact velocities, theoretically separating the three deformation regimes of cellular materials, were estimated using the constitutive R-PLH model [7] based on the results of the quasi-static compression experiments reported in the previous section. A comparison of the predicted engineering stress-strain relationships from the R-PLH model to the experimental results is presented in Fig. 9 and demonstrates a good match. The calculation of two critical velocities yielded values of 15.7 and 29 m/s. It is expected that impact velocities below 15.7 m/s (0.1 mm/s and 14 m/s) will fall within the quasi-static loading regime, velocities between 15.7 and 29 m/s (25 m/s) will fall within the dynamic transitional regime, and velocities above 29 m/s (55, 75, and 95 m/s) will fall within the shock regime.

3.2.2. *Dynamic loading*

The initial impact velocities and their corresponding average values for all DIHB experiments, determined using the DIC method, are listed in Table 5. For simplicity, each group of initial velocities was referred to using the average value.

The DIC method was also used to determine the striker velocity profiles after the initial impact, shown in Fig. 10. A continuous deformation pulse is necessary for an experiment to be considered as having a constant impact. This is achieved by maintaining a constant velocity profile. In all tests, a constant velocity plateau was observed during the entire deformation process until the densification, when the striker velocity dropped sharply due to the inertia of the fully compressed specimens and the incident bar. The most pronounced constant velocity plateau was observed at 14 m/s, Fig. 10. The plateau duration was shorter in experiments with higher initial impact velocities due to higher strain rates, which made the plateau regions less pronounced when viewed on a graph's time scale.

At an impact velocity of 14 m/s, the first structural collapses occur at the weakest points of the cellular material, as shown in Fig. 11a. The formation of a deformation front is illustrated by the red dashed line, and the red arrows indicate the direction of the impact. In this case, the deformation front moved from the opposite end to the impact end of the specimen, as shown by the grey line on the right side of each deformation sequence in Fig. 11. This homogeneous deformation mode defines a quasi-static loading regime, where cells deform by bending and collapsing cell walls until adjacent walls come into contact, and then begin to collapse, which marks the beginning of the densification phase. This deformation mode was present at both 0.1 mm/s and 14 m/s.

Fig. 11b shows the deformation sequence of the test specimen at an impact velocity of 25.9 m/s. The deformation was initially a combination of deformations at the weakest locations and on the impact side of the specimen. The deformation front later occurred at the opposite end of the specimen and then moved towards the impact end. Again, irregular cell collapses in the weakest locations were observed. This deformation type is common in the transitional loading regime.

A localised layerwise deformation across the specimen was observed at impact velocities of 55.7, 76, and 93.6 m/s. This deformation is typical of the shock loading regime. The deformation front appeared at the impact end of the specimen and propagated to the opposite end (Fig. 11c). In this case, the cells behind the deformation front were fully crushed. In contrast, the cells in front of the deformation front remain completely undeformed until all the cells in the layer collapse. This deformation mode is a result of the inertial effect, which determines the deformation mechanisms at the macro level. The deformation front has a one-layer cell size.

As previously mentioned, the quasi-static loading regime was observed at loading velocities of 0.1 mm/s and 14 m/s, which corresponds well with the analytical predictions of the R-PLH model for the quasi-static loading regime to be present under the first critical velocity of 15.7 m/s. A transitional loading regime was observed at a velocity of 25.9 m/s, which also aligns well with the R-PLH model prediction. The highest shock loading regime was dominant at velocities of 55.7, 76, and 93.6 m/s, as predicted by the second critical velocity of 29 m/s.

The deformation behaviour of the foam is depicted through an engineering stress-strain relationship for all loading regimes in Fig. 12. The relationship demonstrates an increase in stress response as the strain rate increases, which is a result of the influence of inertia in the dynamic loading regime. The strain rate hardening phenomenon demonstrates that the material's strength and resistance to deformation

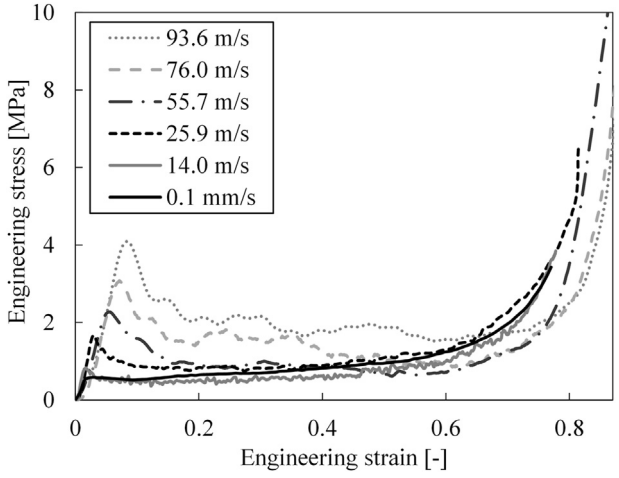

Fig. 12 – Average engineering stress-strain curves at different initial impact velocities.

Table 6 – Evaluated mechanical parameters at different loading rates.

Loading rate	Velocity [m/s]	PS [MPa]	σ_p [MPa]	σ_d [MPa]	ε_d [–]	SEA [J/g]
Q-S	0.0001	0.58	0.72	0.93	0.50	2.08
DYN	14.0	0.83	0.57	0.74	0.5	1.62
	25.9	1.67	0.83	1.08	0.5	2.75
	55.7	2.27	0.89	1.15	0.69	3.95
	76.0	3.08	1.59	2.06	0.78	6.76
	93.6	4.09	1.95	2.54	0.80	9.73

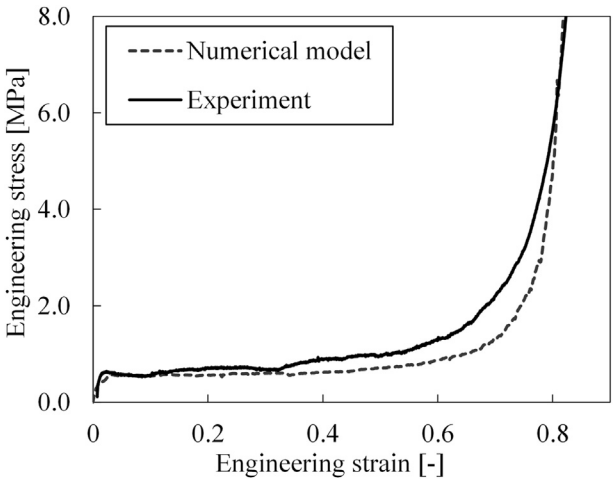

Fig. 13 – Comparison of quasi-static experimental and computational results for S1 specimen at the loading velocity of 0.1 mm/s.

increase as the strain rates rise. This effect is attributed to the rapid deformation occurring within a short time period, which restricts the material's microstructure from rearranging and leads to enhanced resistance against further deformation. The significance of the inertial effect becomes more prominent as the strain rate increases, contributing significantly to the high strain hardening effect. The rapid acceleration induces high strain rates, resulting in profound plastic deformation. Consequently, this rapid deformation, in combination with the strain hardening effect, leads to enhanced strength and altered mechanical properties of the open-cell foam. The evaluated mechanical parameters for the quasi-static (Q-S) and dynamic (DYN) loading regimes were determined from the calculated stress-strain relationships in Fig. 12 and are presented in Table 6. It is evident that an increase in the impact velocity causes an increase of the peak stress PS, larger stress drops to a plateau stress σ_p thereafter and an increase of the densification strain ε_d and stress σ_d, all resulting in a significant increase in the SAE. When comparing the lowest (0.1 mm/s) and the highest (93.6 m/s) loading velocity, the average increase in PS, σ_p, and SEA factor was 86%, 63%, and 79%, respectively.

There was a strong correlation between the results at velocities of 0.1 mm/s and 14 m/s, as both cases fall under the same quasi-static loading regime. The stress gradually increases until the densification strain after the initial yielding of the weakest cells in the foam specimens at a test velocity of 0.1 mm/s. A typical increase in PS was observed at an impact velocity of 14 m/s during the DIHB test, although the observed deformation regime was still quasi-static. The plateau stress, densification stress at the same densification strain and SEA are interestingly slightly smaller than one measure for the test velocity 0.1 mm/s. This is attributed to a more brittle failure of foam struts at higher loading velocity conditions.

A higher PS, plateau stress, densification stress and SEA increase were observed in the transitional loading regime at 25.9 m/s, with the same densification strain as in the quasi-static loading regime. An average increase of 24% in the SEA parameter was observed.

In the shock loading regime at velocities of 55, 76, and 93.6 m/s, a significant increase in the PS, plateau stress, densification stress and strain and SEA proportional to higher strain rates were observed. Slightly larger stress oscillations were detected compared to the quasi-static and transitional loading regimes. These stress oscillations were caused by the deformation of individual cells and the propagation of stress waves in the already densified layers of the foam. As the deformation rate increases, the stresses in the plateau region also increase. Larger densification strains and, consequently, longer plateau stages were measured. As the densification stress and strain increased, the open-cell foam was able to absorb more energy, resulting in an increased SEA factor. In summary, the mechanical response of the open-cell

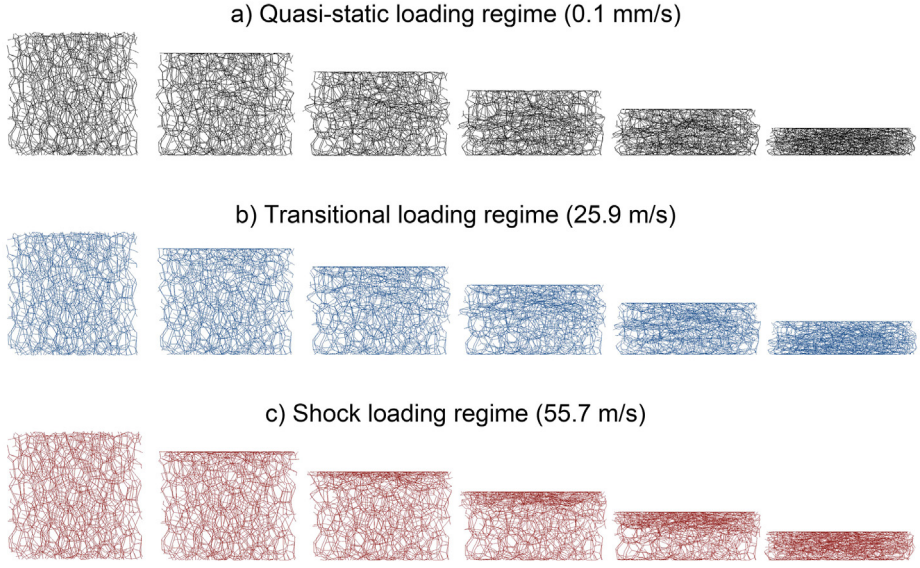

Fig. 14 – Deformation behaviour of open-cell numerical model S1 under different loading regimes at the deformation step of 12.5%.

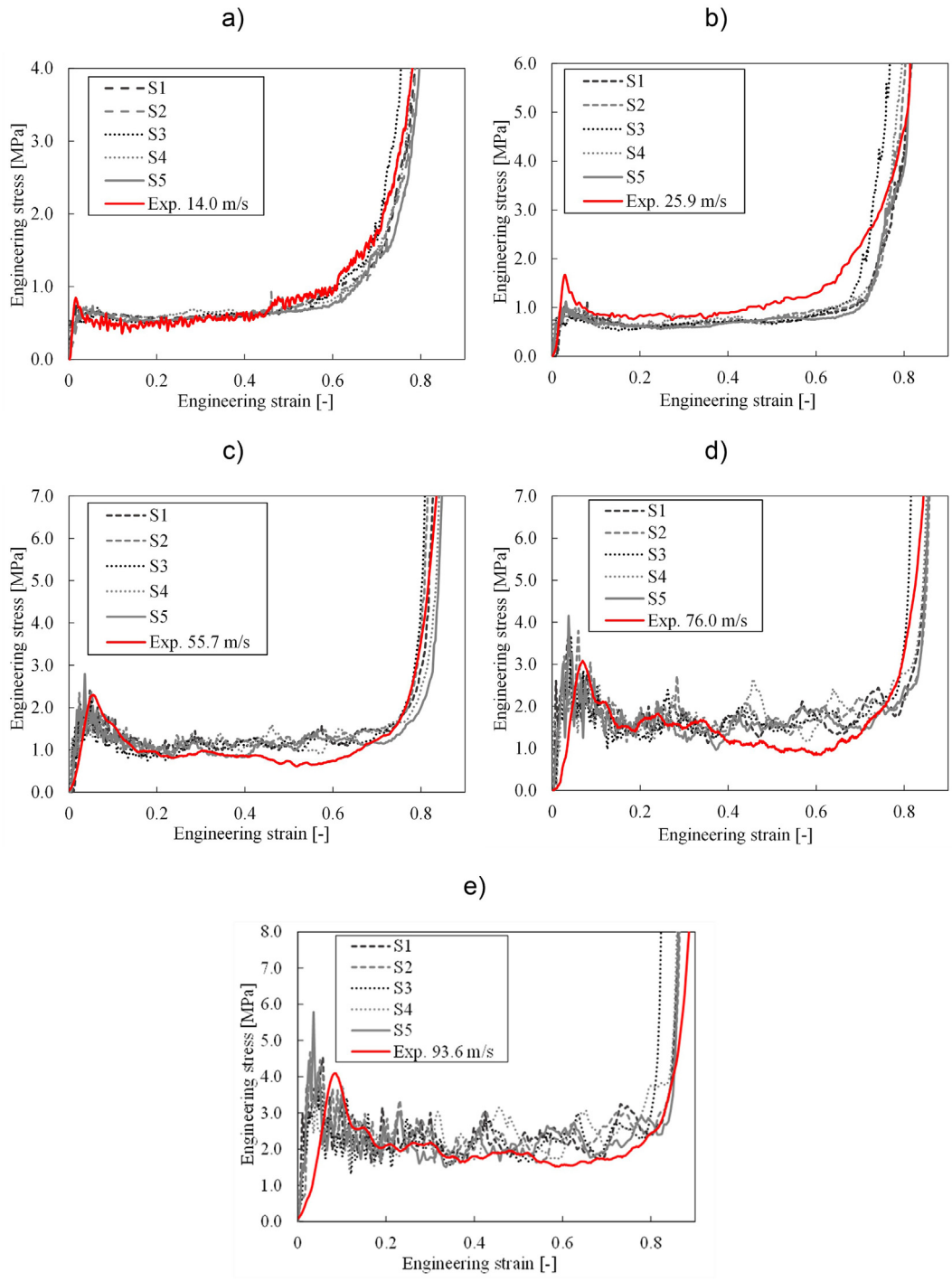

Fig. 15 – Comparison of experimental and computational results at a) 14, b) 25.9, c) 55.7, d) 76, and e) 93.6 m/s.

aluminium foam was improved regarding SEA with increasing strain rate.

3.3. *Computational results*

Five numerical models were constructed using open-cell foam geometries S1–S5, obtained through mCT scans. The models were initially validated by comparing the computational results to the experimental results at a quasi-static loading velocity of 0.1 mm/s. Fig. 13 shows a relatively good agreement between measured and computed engineering stress-strain relationships of specimen S1. The experimental stress values were slightly higher than computed values at higher strains, as expected due to the use of the simplified numerical model.

The behaviour of the open-cell foam at higher strain rates was simulated using numerical models with the added Cowper-Symonds strain-rate-dependent material model. Fig. 14 shows the deformation process of numerical model S1 in all loading regimes. The computational simulations

Table 7 – Comparison of experimental (E) and computational (C) mechanical parameters at different loading rates.

Velocity [m/s]	0.0001		14		25.9		55.7		76.0		93.6	
	E	C	E	C	E	C	E	C	E	C	E	C
PS [MPa]	0.58	0.53	0.83	0.65	1.67	0.90	2.27	1.98	3.08	2.92	4.09	3.62
σ_p [MPa]	0.72	0.57	0.57	0.59	0.83	0.69	0.89	1.08	1.59	1.56	1.95	2.14
σ_d [MPa]	0.93	0.74	0.74	0.77	1.08	0.89	1.15	1.40	2.06	2.02	2.54	2.79
ε_d [–]	0.50	0.53	0.50	0.5	0.50	0.61	0.69	0.72	0.78	0.74	0.80	0.80
SEA [J/g]	2.08	1.73	1.62	1.82	2.75	2.63	3.95	5.28	6.76	7.50	9.73	11.40

observed the same deformation mechanisms as in the experimental tests. At a low deformation rate in the quasi-static regime (0.1 mm/s and 14 m/s), the first deformation occurred at the weakest locations in the open-cell structure, consequently forming a deformation front progressing towards both ends of the specimen.

The deformation mode at 25.9 m/s was a combination of deformations at the weakest locations and on the impact side of the specimen. They corresponded well with the experimentally observed deformation mode in the transitional regime, Fig. 14b. In this regime, the deformation front had not yet spread throughout the entire cross-section of the specimen, leaving some cells undamaged in front and behind the deformation front. These undamaged cells eventually collapsed in the last phase of densification.

The response of materials to shock loading is influenced by various factors, in solid materials primarily by the modulus of elasticity, density, and the specific stress-strain behavior of the base material. The shock loading is characterised by shock compression wave propagating through the material at very high speed, initiated by impacting body at higher impact speed. The speed of shock wave propagation in cellular materials depends also on the structural geometry, including distinct deformation patterns and failure modes. Since the open-cell materials are highly porous with diverse structural geometry, the shock wave is in these materials mostly driven by layer wise collapse and consecutive layer by layer densification of the cellular structure away from the impact area, as shown in Fig. 14c. This leads to significantly lower shock loading velocities as discussed in Ref. [7]. The estimated second critical velocity of the tested material, separating the intermediate and shock deformation regimes, is 29 m/s. The testing velocity of 55.7 m/s is well above the second critical velocity and a localized deformation front characterized by a narrow region encompassing a single layer of cells experiencing significant deformation until full densification is observed, Fig. 14c. This front then propagates to the next cell layer and the process repeats itself until full sample densification. This phenomenon is consistent with experimental observations.

Furthermore, the stress-strain response provides evidence of the achieved shock mode in the open-cell foam, as illustrated in Fig. 15. Stress values in the numerical simulations are significantly lower at velocities below 55.7 m/s compared to higher testing velocities.

Fig. 15 compares the experimental and computational engineering stress-strain relationships at different impact velocities. The quantitative comparison of the average measured and computed mechanical parameters for all analysed impact velocities is presented in Table 7. The results were in good agreement at an impact velocity of 14 m/s. However, there were some deviations at a higher velocity of 25.9 m/s. The numerical model featured thinner cell ligaments with a smaller cross-section, leading to lower plateau stresses and PS values than the experimental results. The numerical models showed higher stress oscillations in the plateau region at impact velocities in the shock loading regime. These oscillations were also present in the experimental results but were more pronounced in the computational results due to failure modelling effects. However, the numerical models could represent the responses of the five analysed specimens (S1–S5) accurately enough, despite the inherent inhomogeneity of the open-cell foam's internal structure. The maximum deviation of the SEA factor between experimental and computationally predicted values was 16% or less on average.

The overall agreement between the computational and experimental results was deemed good enough for fast estimating aluminium foam mechanical response to different loading regimes.

4. Conclusions

This study aimed to comprehensively characterise the open-cell aluminium foam M-pore® under various loading velocities. This was achieved by conducting experiments at loading velocities of 0.1 mm/s, 14, 25.9, 55.7, 76, and 93.6 m/s. The experiments were carried out using a servo-hydraulic Instron testing device for quasi-static loading and a modified DIHB set-up for higher-speed loading. The DIC method was used to precisely determine the initial impact velocity and evaluate the velocity profile from high-resolution digital deformation images. The constant velocity profile observed in all experiments confirmed the suitability of the DIHB set-up. The constitutive R-PLH model based on quasi-static testing results of aluminium foam samples was used to theoretically predict two critical loading velocities, 15.7 and 29 m/s, separating the quasi-static, intermediate and shock loading regimes. Quasi-static loading regime occurred at the testing velocity of 0.1 mm/s and 14 m/s, the transitional regime at 25.9 m/s, and the shock regime at a velocity of 55.7 m/s and above.

The results showed that the material's response improved with increasing strain rates, as evidenced by an increase in PS by 86%, σ_p by 63%, and the SEA factor by 79% when comparing the lowest and highest impact velocities. In the quasi-static regime, the first collapses occurred at the weakest points of the cellular material, and the deformation front propagated

from the opposite to the impact end of the specimen in the form of typical deformation bands. The deformation mechanism in the transitional regime was initially a combination of deformations at the weakest locations and on the impact side of the specimen. The deformation front later occurred at the opposite end of the specimen and then moved towards the impact end. A localised layer-wise deformation across the specimen was pronounced in the shock regime, with a clear deformation front appearing at the impact end of the specimen and propagating to the opposite end.

The mCT images were used to build simplified 3D numerical models of analysed aluminium foam specimens that were used in fast computational simulations of their behaviour under all experimentally tested loading regimes. The overall agreement between the experimental and computational results was good enough to validate the built numerical models capable of correctly simulating the mechanical response of analysed aluminium foam at different loading rates.

Based on the findings and methodology described in the text, there are several potential areas for future work. Firstly, expanding the investigation to include higher impact velocities could provide insights into the foam's behavior under extreme loading conditions. Secondly, incorporating advanced imaging techniques, such as in-situ imaging during loading, would capture the foam's dynamic response at a finer scale. Additionally, integrating multi-scale modelling techniques could help establish a link between microstructural features and macroscopic mechanical properties, enhancing the understanding of the foam's response under different loading regimes. The combination of experimental data and computational simulations would contribute to a more comprehensive understanding of the material's behaviour.

Data availability

The data that support the findings of this study are available on request from the corresponding author.

Declaration of competing interest

The authors declare that they have no known competing financial interests or personal relationships that could have appeared to influence the work reported in this paper.

Acknowledgements

The authors acknowledge the financial support from the Slovenian Research Agency (national research programme funding No. P2-0063). The authors also acknowledge the help with quasi-static experiments of Prof. dr. Lovre Krstulović-Opara at the Faculty of Electrical Engineering, Mechanical Engineering and Naval Architecture, University of Split, Split, Croatia. The authors acknowledge the support by the projects UIDB/00481/2020 and UIDP/00481/2020 - Fundação para a Ciência e a Tecnologia; and CENTRO-01-0145-FEDER-022083 - Centro Portugal Regional Operational Programme (Centro2020), under the PORTUGAL 2020 Partnership Agreement, through the European Regional Development Fund.

REFERENCES

[1] Duarte I, Vesenjak M, Krstulović-Opara L. Dynamic and quasi-static bending behaviour of thin-walled aluminium tubes filled with aluminium foam. Compos Struct 2014;109(1):48–56. https://doi.org/10.1016/J.COMPSTRUCT.2013.10.040.

[2] Fíla T, et al. Strain dependency of Poisson's ratio of SLS printed auxetic lattices subjected to quasi-static and dynamic compressive loading. Adv Eng Mater Aug. 2019;21(8):1900204. https://doi.org/10.1002/adem.201900204.

[3] Šleichrt J, et al. Dynamic penetration of cellular solids: experimental investigation using Hopkinson bar and computed tomography. Mater Sci Eng, A Jan. 2021;800:140096. https://doi.org/10.1016/J.MSEA.2020.140096.

[4] Mauko A, et al. Dynamic deformation behaviour of chiral auxetic lattices at low and high strain-rates. Metals Dec. 2020;11(1):52. https://doi.org/10.3390/met11010052.

[5] Sun Y, Li QM. Dynamic compressive behaviour of cellular materials: a review of phenomenon, mechanism and modelling. Int J Impact Eng Feb. 2018;112:74–115. https://doi.org/10.1016/J.IJIMPENG.2017.10.006.

[6] Sun Y, Li QM, Lowe T, McDonald SA, Withers PJ. Investigation of strain-rate effect on the compressive behaviour of closed-cell aluminium foam by 3D image-based modelling. Mater Des Jan. 2016;89:215–24. https://doi.org/10.1016/J.MATDES.2015.09.109.

[7] Ding Y, Wang S, Zheng Z, Yang L, Yu J. Dynamic crushing of cellular materials: a unique dynamic stress–strain state curve. Mech Mater Sep. 2016;100:219–31. https://doi.org/10.1016/J.MECHMAT.2016.07.001.

[8] Duarte I, Vesenjak M, Krstulović-Opara L. Variation of quasi-static and dynamic compressive properties in a single aluminium foam block. Mater Sci Eng, A 2014;616:171–82. https://doi.org/10.1016/j.msea.2014.08.002.

[9] Liang M, Li Z, Lu F, Li X. Theoretical and numerical investigation of blast responses of continuous-density graded cellular materials. Compos Struct 2017. https://doi.org/10.1016/j.compstruct.2016.12.065.

[10] Zheng Z, Yu J, Wang C, Liao S, Liu Y. Dynamic crushing of cellular materials: a unified framework of plastic shock wave models. Int J Impact Eng Mar. 2013;53:29–43. https://doi.org/10.1016/J.IJIMPENG.2012.06.012.

[11] Borovinšek M, Vesenjak M, Jože M, Ren Z. Computational reconstruction of scanned aluminum foams for virtual testing. J Serbian Soc Comput Mech 2008;2(2):16–28.

[12] Borovinšek M, Ren Z. Computational modelling of irregular open-cell foam behaviour under impact loading. Mater Werkst Feb. 2008;39(2):114–20. https://doi.org/10.1002/MAWE.200700270.

[13] Vesenjak M, Veyhl C, Fiedler T. Analysis of anisotropy and strain rate sensitivity of open-cell metal foam. Mater Sci Eng, A Apr. 2012;541:105–9. https://doi.org/10.1016/J.MSEA.2012.02.010.

[14] Huluka S, Abdul-Latif A, Baleh R, Larbi A, Deiab I, Khanafer K. Biaxial characterization of open-cell aluminum foams from macro to micro responses. Mater Sci Eng Mar. 2023;868. https://doi.org/10.1016/j.msea.2023.144588.

[15] Zhao S, Zhang X, Wang R, Li R. Stress-strain states and energy absorption in open-cell aluminium foams under hypervelocity impact. Compos Struct Jun. 2023:116885. https://doi.org/10.1016/j.compstruct.2023.116885.

[16] Rahimidehgolan F, Altenhof W. Compressive behavior and deformation mechanisms of rigid polymeric foams: a review," *Composites Part B: engineering*, vol. 253. Elsevier Ltd; Mar. 15 2023. https://doi.org/10.1016/j.compositesb.2023.110513.
[17] Chen W, Song B. Split Hopkinson (Kolsky) Bar Design, Testing and Application 2008;39(5).
[18] Neuhäuserová M, et al. Strain rate-dependent compressive properties of bulk cylindrical 3D-printed samples from 316L stainless steel. Materials Feb. 2022;15(3). https://doi.org/10.3390/MA15030941.
[19] Jing L, Wang Z, Ning J, Zhao L. The dynamic response of sandwich beams with open-cell metal foam cores. Compos B Eng Jan. 2011;42(1):1–10. https://doi.org/10.1016/j.compositesb.2010.09.024.
[20] Shunmugasamy VC, Mansoor B. Compressive behavior of a rolled open-cell aluminum foam. Mater Sci Eng Feb. 2018;715:281–94. https://doi.org/10.1016/j.msea.2018.01.015.
[21] Xiao-qing Cao, Wang Zhi-hu, Hong-wei Ma, Zhao Long-ma, Gui-tong Yang. Effects of cell size on compressive properties of aluminum foam. Science Press; 2006. p. 351–6 [Online]. Available: www.sciencedirect.comwww.csu.edu.cn/ysxb/.
[22] Fíla T, et al. Impact behavior of additively manufactured stainless steel auxetic structures at elevated and reduced temperatures. Adv Eng Mater Jan. 2021;23(1):2000669. https://doi.org/10.1002/ADEM.202000669.
[23] Curry RA, Govender RJ. The 'Open' Hopkinson pressure bar : towards addressing force equilibrium in specimens with non-uniform deformation. Journal of Dynamic Behavior of Materials 2016;2(1):43–9. https://doi.org/10.1007/s40870-015-0042-2.
[24] Couque H. The use of the direct impact Hopkinson pressure bar technique to describe thermally activated and viscous regimes of metallic materials. Phil Trans Math Phys Eng Sci Aug. 2014;372(2023):20130218. https://doi.org/10.1098/rsta.2013.0218.
[25] Lopatnikov SL, et al. Dynamics of metal foam deformation during Taylor cylinder-Hopkinson bar impact experiment. Compos Struct 2003;61(1–2):61–71. https://doi.org/10.1016/S0263-8223(03)00039-4.
[26] Banhart J. Manufacture, characterisation and application of cellular metals and metal foams. Prog Mater Sci 2001. https://doi.org/10.1016/S0079-6425(00)00002-5.
[27] Sun Y, Li QM. Dynamic compressive behaviour of cellular materials: a review of phenomenon, mechanism and modelling. Int J Impact Eng Feb. 2018;112:74–115. https://doi.org/10.1016/J.IJIMPENG.2017.10.006.
[28] Sarıkaya M, Taşdemirci A, Güden M. Dynamic crushing behavior of a multilayer thin-walled aluminum corrugated core: the effect of velocity and imperfection. Thin-Walled Struct Nov. 2018;132:332–49. https://doi.org/10.1016/j.tws.2018.06.029.
[29] Couque H. The use of the direct impact Hopkinson pressure bar technique to describe thermally activated and viscous regimes of metallic materials. Phil Trans Math Phys Eng Sci Aug. 2014;372(2023):20130218. https://doi.org/10.1098/rsta.2013.0218.
[30] Adorna M, Bronder S, Falta J, Zlámal P, Fíla T. Evaluation of Hopkinson bar experiments using multiple digital image correlation software tools. In: 17th youth symposium on experimental solid Mechanics, YSESM 2019, vol. 25; Dec. 2019. p. 1–5. https://doi.org/10.14311/APP.2019.25.0001.
[31] Hallquist J. LS-DYNA keyword user's manual. Livermore, California: Livermore Software Technology Corporation; 2007.
[32] Borovinšek M, Vesenjak M, Hokamoto K, Ren Z. An experimental and computational study of the high-velocity impact of low-density aluminum foam. Materials 2020;13:1949. https://doi.org/10.3390/MA13081949. 13, no. 8, p. 1949, Apr. 2020.
[33] Reid SR, Peng C. Dynamic uniaxial crushing of wood. Int J Impact Eng May 1997;19(5–6):531–70. https://doi.org/10.1016/S0734-743X(97)00016-X.